Core–shell structured iron nanoparticles well dispersed on montmorillonite

Mingde Fan [a,b], Peng Yuan [a,*], Jianxi Zhu [a], Tianhu Chen [c], Aihua Yuan [d], Hongping He [a,**], Kangmin Chen [e], Dong Liu [a,b]

[a] Guangzhou Institute of Geochemistry, Chinese Academy of Sciences, Guangzhou 510640, PR China
[b] Graduate School of the Chinese Academy of Science, Beijing 100039, PR China
[c] School of Resources and Environmental Engineering, Hefei University of Technology, Hefei 230009, PR China
[d] School of Material Science and Engineering, Jiangsu University of Science and Technology, Zhenjiang 212003, PR China
[e] School of Material Science and Engineering, Jiangsu University, Zhenjiang 212003, PR China

ARTICLE INFO

ABSTRACT

Iron nanoparticles have been successfully synthesized using sodium borohydride solution reduction of ferric trichloride hexahydrate in the presence of montmorillonite as an effective protective reagent and support as well. A combination of characterizations reveals the well disperse of these obtained iron nanoparticles supported on the external surface of clay with roughly spherical morphology and mean diameter of 55 nm. The particles are oxidation resistant well with iron core–iron oxide shell structure. The shell thickness of 3 nm remains almost invariable under ambient conditions. Discernable hysteresis loop reveals ferromagnetic behavior of the iron nanoparticles, which make them easy for magnetic separation and potential in some practical applications.

© 2009 Elsevier B.V. All rights reserved.

1. Introduction

Novel quantum size-dependent physicochemical properties make metallic iron nanoparticles of great potential in a wide range of applications including magnetic recording media [1], ferrofluids [2], magnetic resonance imaging contrast agents [3], heterogeneous catalysts [4], and environment remediation [5–7]. Different strategies have been so far reported for synthesizing iron nanoparticles. Chemical reduction of iron salts with borohydrides in solution among these reported methods shows some prominent advantages such as safety, simplicity, low cost, and feasibility in most laboratories. However, a disadvantage of this method is that the iron product strongly depends on the preparation conditions. Almost any changes in the preparation procedure might have obvious influences on the resultant product. In addition, this method is prone to introduce impurity of boron into iron product. For example, some previous studies have revealed the occurrence of the invasion of boron invading into iron crystal lattice [8,9]. The borohydride reduction method is also limited by ease to oxidize and addiction to aggregate of iron nanoparticles.

The oxidation of iron nanoparticles is conventionally minimized under vacuum condition or in inert atmosphere. Attempts

to form shell coating iron core have also been applied to protect the iron core from further oxidation. The shell can be composed of different materials, among which the native iron oxide is attractive and intensively studied for its almost unavoidable formation and high efficiency to suppress oxidation of iron core [10–13]. The aggregation of iron nanoparticles can be largely inhibited by dispersing them with organic or inorganic protective reagents. Compared with polymer or surfactant protective reagents, inorganic chemically inert ones such as clay minerals are more cost-effective and environment-friendly. Furthermore, they can also act as supports to facilitate reuse and recycling of nanoparticles. Of such clay minerals, montmorillonite (Mt) is often used as an effective protective reagent and support as well. Mt is a naturally occurring 2:1 type layered alumonosilicate with turbostratic structure [14], in which each layer comprises an alumina octahedral sheet sandwiched between two silica tetrahedral sheets, and the layer has a permanent negative charge resulting from isomorphous substitution occurring mainly in the octahedral sheet. Such layers are stacked by weak dipolar or Van der Waals forces, leading to the intercalation of charge compensating cations into the interlayer space and causing Mt to be easily expanded along the c-direction. Therefore, not only adsorption on the external surface but also intercalation into the interlayer space can occur [15]. Accordingly, in the case of nanoparticles generation using the borohydride reduction method, two reaction sites from the external surface and the interlayer space are available in Mt. Many efforts for synthesizing nanoparticles by borohydride

---

* Corresponding author. Tel.: +86 20 85290341; fax: +86 20 85290130.
** Corresponding author. Tel.: +86 20 85290257; fax: +86 20 85290130.
E-mail addresses: yuanpeng@gig.ac.cn (P. Yuan), hehp@gig.ac.cn (H. He).

reduction resort to Mt to inhibit particle agglomeration and to act as a support. However, might be due to the complications of the borohydride reduction method itself, few studies as we know are available related to the generation of iron nanoparticles using borohydride solution reduction in the presence of Mt.

Here we present our results obtained from synthesizing nanoscale metallic iron nanoparticles well dispersed on Mt using sodium borohydride reduction in solution. The iron core–iron oxide shell structure of the resultant particles and their magnetic behavior are also investigated.

2. Experimental

Raw Mt sample obtained from Inner Mongolia, China was purified by sedimentation and the fraction less than 2 μm was collected. The Mt fine fraction was then ion-exchanged with NaCl solution to obtain Na^+–montmorillonite (Na^+–Mt). Some Mt fine fraction (6 g) was dispersed in 400 ml aqueous acetone solution (50% v/v) and then treated with 600 ml aqueous NaCl solution (0.2 M) at 80 °C for 24 h according to the literature method [15] with some modifications. The cationic exchange capacity (CEC) of these obtained Na^+–Mt was determined according to the ammonium acetate saturation method [16] and was found to be 111.1 mmol/100 g. The Na^+–Mt was used as protective reagent and support for the synthesis of iron nanoparticles. $FeCl_3 \cdot 6H_2O$ and $NaBH_4$ available locally were all of analytical grade and used as received. Distilled water was used throughout this work.

Iron nanoparticles were synthesized using the modified version of Wang and Zhang [5]. Typically, Na^+–Mt (1.0 g) was stirred in 50 ml water for 24 h, then $FeCl_3 \cdot 6H_2O$ (corresponding to 6 CEC of Na^+–Mt) was added to the aqueous clay suspension. The mixture was stirred for another 24 h and then 50 ml freshly prepared $NaBH_4$ solution was dropwise added under stirring. The molar ratio of borohydride to ferric iron was 4:1. After $NaBH_4$ was added the solution turned to black, indicating the reduction of ferric iron. All the experiments were carried out at room temperature and no precautions were taken to eliminate oxygen from the reaction vessel. After several centrifugation/redispersion cycles in 50% v/v aqueous ethanol solution then in acetone, the final product was vacuum dried at 60 °C for 24 h. Reference iron particles were prepared with the same procedure mentioned above except the absence of clay.

Element analyses were performed on a Varian Vista-Pro inductively coupled plasma optical emission spectrometry (ICP-OES). Crystal phases were identified by X-ray diffraction (XRD) with a Bruker D8 Advance diffractometer using CuKα radiation. Microstructure characterization and particle size determination were carried out by a combination of a 100 kV JEOL JEM-100CXII transmission electron microscope (TEM) attached an electron diffractometer, a 200 kV JEOL JEM-2100 high-resolution transmission electron microscope (HRTEM), and a 5 kV FEI-Sirion 200 field emission scanning electron microscope (FESEM) attached an Oxford INCA energy dispersive X-ray spectroscopy (EDX). Magnetic behavior was measured using a Quantum Design MPMS superconducting quantum interference device (SQUID) magnetometer.

3. Results and discussion

The reference iron nanoparticles generated in homogeneous solution in the absence of Mt are roughly spherical and connected in chains of about 80 nm in width as shown in Fig. 1a. The chain-like morphology of iron particles caused by magnetostatic attraction are also reported in literature [17,18]. The α-Fe phase present in the XRD pattern (Fig. 2a) reveals the metallic nature of the particles, and the existence of iron oxide is also observed. This indicates the existence of the iron core–iron oxide shell structure of the reference particles. The iron oxide might be magnetite and/or maghemite. The two oxides have similar lattice constants. So, they are not easily distinguished by XRD. Exact identification of the two oxide phases by Mössbauer spectroscopy is being conducted.

No boron is detected by EDX analysis as shown in Fig. 1b. The absence of boron signal may be due to the trace amount or the separating state of the element. The lattice constant of the reference iron $a = 2.866$ Å, refined by least square fit following the TREOR algorithm, shows negligible variation to the reported value of bcc structured α-Fe (JCPDS No. 06-0696). This coincidence prefers that boron segregates in a separating state from the iron product. Similar result has also been reported by Corrias et al. [19]. As mentioned above, some previous studies have revealed the possibility of boron invading into the crystal lattice of iron [8,9]. The difference between this study and the previous ones might be attributed to the different experimental conditions adopted, respectively. In particular, we adopted the borohydride to iron molar ratio of 4:1 as recommended by Wang and Zhang [5], which is suitable for generating iron nanoparticles. The ratio of 4:1 adopted in this study is less than that adopted by Zhang and Manthiram [8]. In their study a borohydride to iron molar ratio of about 12:1 was adopted, if the Mt CEC value could be considered as 100 mmol/100 g typical for this type of clay. The decrease of the ratio indicates less borohydride used in this study, which might reduce the chance of boron incorporating into iron crystal lattice. The iron and oxygen signals in the EDX analysis are from the
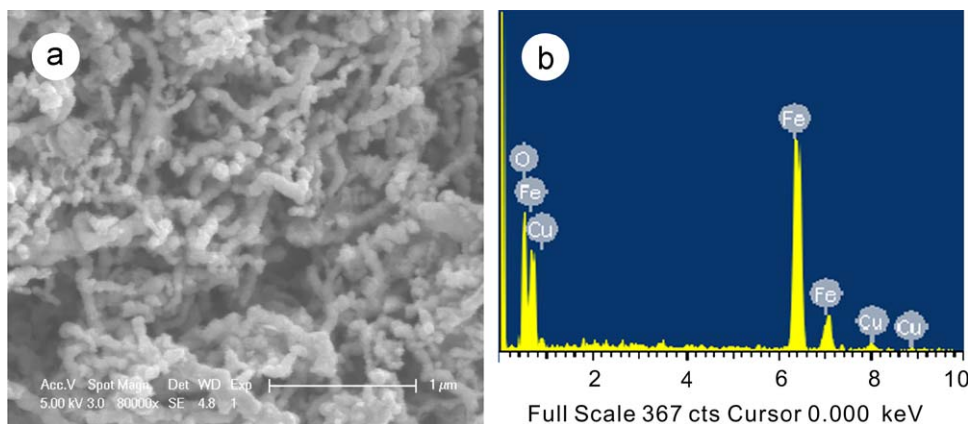

Fig. 1. (a) FESEM image of iron nanoparticles obtained using borohydride solution reduction of ferric iron salt in the absence of montmorillonite. Chain-like morphology from magnetostatic attraction of the particles is clearly revealed. EDX result is shown in (b).

resultant iron particles, and the copper signal from copper conductive tape (Fig. 1b).

Fig. 3 shows microscopy overview of the iron particles obtained by borohydride solution reduction of ferric iron salt in the presence of Na$^+$–Mt as a protective reagent and support as well. The well disperse of the roughly spherical particles is clearly
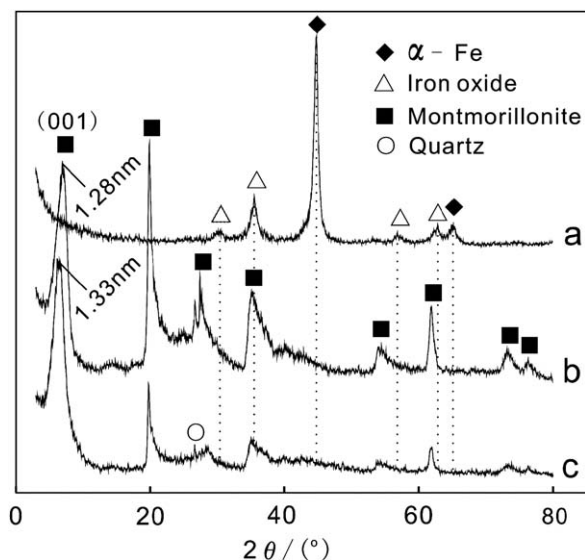

Fig. 2. XRD pattern of (a) clay free and (c) clay supported iron nanoparticles obtained using borohydride solution reduction of ferric iron salt without and with montmorillonite, respectively. In (b) is XRD pattern of Na$^+$–Mt.

revealed by both the low-magnification TEM and FESEM observations shown in Fig. 3a and c, respectively. The particle size distribution (Fig. 3d) fitted with normal function is obtained by sampling a minimum of 300 particles from the TEM images of the product, which gives an mean particle diameter with standard deviation (Std. Dev. in abbreviation) of 55 ± 11 nm. The relative standard deviation 0.2, which is obtained by dividing the standard deviation by the mean particle diameter, implies a high monodispersity of the iron particles. In contrast to the chain-like and agglomerate state of the reference particles, the monodispersity is due to the control of nucleation and the prevention of iron cluster–cluster mutual contact by clay. Notably, some short chains and small agglomerations also exist, which might result from the heterogeneous surface activities of the clay used. As shown in Fig. 2b, the Na$^+$–Mt contains minor quartz impurity, and has a $d(0\,0\,1)$ spacing of 1.28 nm. Compared with the Na$^+$–Mt, the $d(0\,0\,1)$ spacing of the clay supported iron product remains almost unchanged at 1.33 nm (Fig. 2c). The basal d spacing of 1.33 nm corresponds to an interlayer height of 0.36 nm, assuming the thickness of the TOT layer of Mt to be 0.97 nm [20]. This limited interlayer height indicates that the iron particles of large size predominantly occupy the external surface of clay. Possibly caused by the fine crystalline size of the iron particles, the XRD pattern of the clay supported iron (Fig. 2c) fails to offer any iron-related information. Substantial evidences for the existence of iron clusters in the interlayer space of clay are still being investigated. The corresponding selected area electron diffraction (SAED) pattern of the product (inset in Fig. 3c) unambiguously shows the presence of α-Fe phase, which can be attributed to the iron cores of the particles. The continuously diffuse diffraction rings reveal the polycrystalline nature of the particles composed
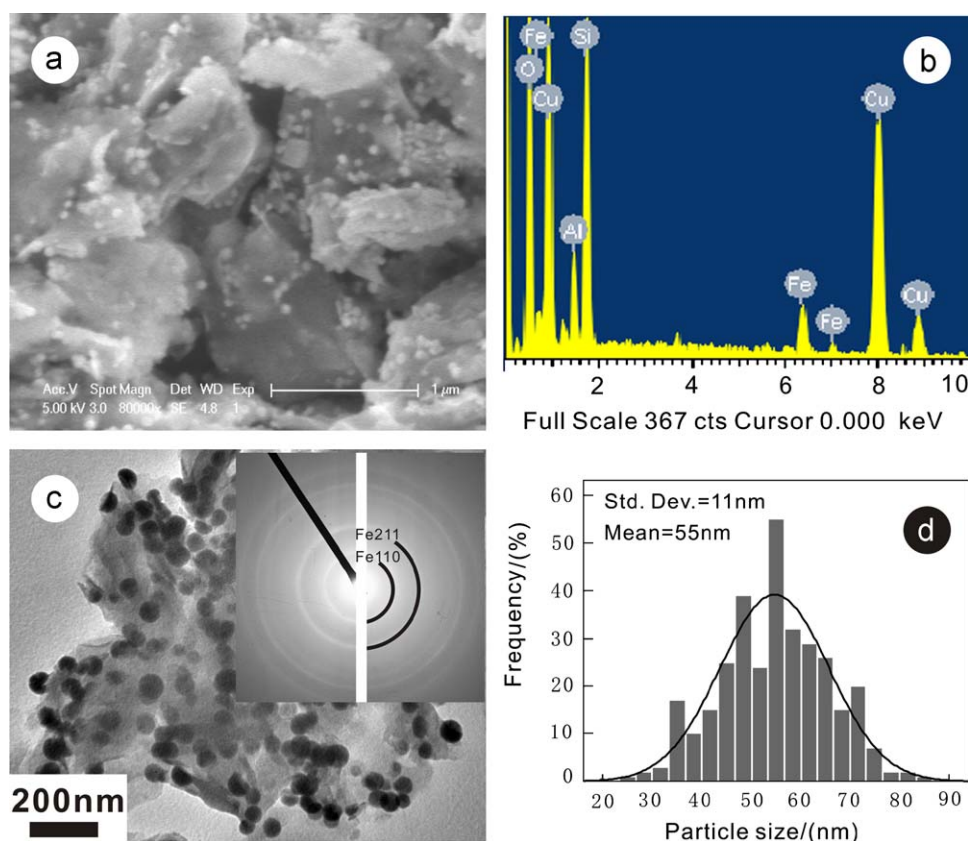

Fig. 3. Overview of iron nanoparticles obtained using borohydride solution reduction of ferric iron salt in the presence of montmorillonite. FESEM and low-magnification TEM images (a and c) show the well disperse of the clay supported iron nanoparticles with size of 55 ± 11 nm indicated by the histogram in (d). SAED pattern inserted in (c) identifies the α-Fe existence. Iron oxides are suggested to occur from the iron and oxygen peaks in EDX spectrum shown in (b).
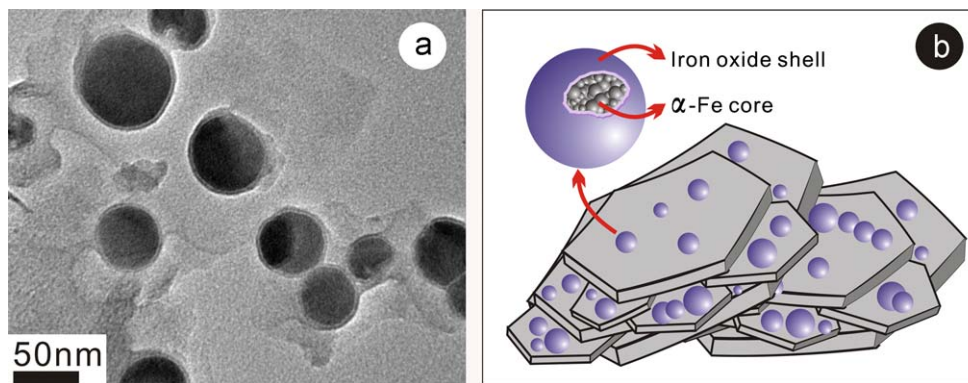
Fig. 4. (a) High-magnification TEM image of iron nanoparticles, the same as in Fig. 3, reveals the core–shell structure with the almost invariable shell thickness of 3 nm independent of the particle size. (b) Schematic representation of the structure characteristics of the clay supported iron nanoparticles.

of fine random-oriented crystal grains, which is coincided with the XRD result. The iron and oxygen peaks in the EDX spectrum (Fig. 3b) reveal the existence of iron oxide shells of the particles, and the absence of boron signal excludes the interference to iron crystal lattice by boron invading as the reference iron particles. The silicon and aluminum peaks are derived from the clay present and the copper peaks from the copper conductive tape (Fig. 3b). These results indicate that the Na^+–Mt used here can act as an effective protective reagent and support for the synthesis of iron nanoparticles with borohydride reduction method. Similar function was also reported for Laponite used in forming gold and silver nanoparticles [21].

High-magnification TEM image (Fig. 4a) clearly shows the different brightness of the clay supported iron nanoparticles with the bright iron oxide shells coating the inner dark iron cores. It is worth noting that the iron oxide shells have an almost invariable thickness of 3 nm independent of the particle size. Shafranovsky and Petrov [12] suggested that fast oxidation of nascent iron powder likely led to form a mixture of magnetite and maghemite. No precautions were taken to eliminate oxygen in the iron generation procedure in this study, which likely causes nascent iron to be fast oxidized and facilitates the formation of iron oxide shell. Combined the existence of iron and oxygen in the EDX analysis (Fig. 3b), the shells of the particles likely comprise magnetite and/or maghemite. Thus, as reported in literature [10,12,13], the Caberra–Mott theory is resorted to describe the oxidation of the iron nanoparticles with almost invariable 3-nm-thick shells. Upon initial attachment of oxygen onto the surface of iron and the formation of a thin oxide layer, the electron tunnels through the thin oxide layer and ionize the oxygen, leading to an electrical field between the iron and the surface of the oxide layer. The electrical field will then drive the outward diffusion of the ionized iron. At room temperature, about 0.2 fs are needed to form an initial 1-nm-thick oxide layer on a freshly exposed iron surface, and 40 s for 2 nm, 40 weeks for 3 nm, 600 years for 4 nm [13,22]. Based on this description our particles are up to now inert with about 3-nm-thick shells. Taking the above arguments into consideration, the structure characteristics of the clay supported iron nanoparticles can be illustrated by the schematic representation shown in Fig. 4b.

In a survey of the magnetic behavior of the clay free and the clay supported iron products, hysteresis loops were recorded at 300 K with a maximum field of 1 T (Fig. 5). Magnetization data of the clay supported iron were normalized by using the net iron content (21% w/w of the sample) obtained from ICP-OES analysis. Both products with α-Fe cores exhibit discernable hysteresis loops indicating the ferromagnetic properties. Considering their larger particle size than the calculated critical size of single domain of α-Fe particles (14 nm [23]), the ferromagnetic properties are understandable. The core–shell structure and some aggregations
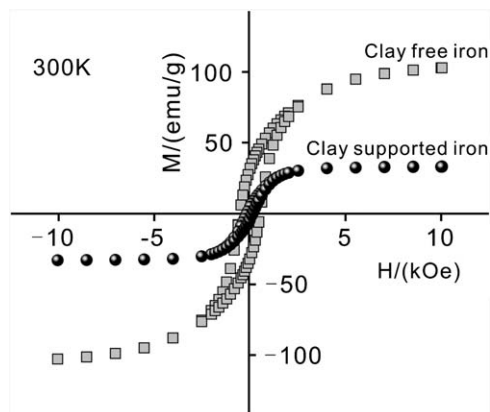

Fig. 5. Magnetization hysteresis loops of clay free and clay supported iron products, recorded at 300 K in a maximum field of 1 T, reveal ferromagnetic behavior for both and the lower magnetic parameters for the clay supported iron than the clay free iron.

also might have contribution to the ferromagnetism. The saturation magnetization (M_s) for bulk iron is 222 emu/g at 298 K [17] while the M_s for the clay free and the clay supported iron are 102 and 33 emu/g, respectively. Clearly, both the clay free and clay supported iron products show much less M_s than that of bulk iron. As indicated by Lai et al. [24] this decrease might be largely due to their small particle size in nanometer scale. With small particle size their magnetic orders are easily randomized and the observed saturation magnetizations are small. The coercivity field (H_c) and the ratio of remnant magnetization (M_r) to M_s (M_r/M_s) of the clay free iron are 541 Oe and 0.31, respectively. Compared with the clay free iron, the H_c and M_r/M_s of the clay supported iron, respectively, reduced to 151 and 0.12. These reductions mainly arise from the confinement of iron particle aggregating. Such confinement effect is reasonably attributed to the clay used as an effective protective reagent, as the role of silica matrix used to enhance the dispersity of iron nanoparticles [25].

4. Conclusions

We have successfully synthesized iron nanoparticles using sodium borohydride solution reduction of ferric iron salt in the presence of Na^+–Mt as an effective protective reagent and support as well. These obtained iron nanospheres with high monodispersity are well dispersed on the external surface of Na^+–Mt and oxidation resistant well with iron core–iron oxide shell structure.

The shell thickness remains almost invariable at 3 nm. The clay supported iron nanoparticles remain ferromagnetic at 300 K, which makes them easy for magnetic separation and potential in some practical applications such as heterogeneous catalysis and environment remediation.

Acknowledgements

References

[1] K. Hayashi, M. Ohsugi, M. Kamigaki, B. Xia, K. Okuyama, Electrochem. Solid-State Lett. 5 (2002) J9.
[2] M.T. López-López, A. Gómez-Ramírez, J.D.G. Durán, F. González-Caballero, Langmuir 24 (2008) 7076.
[3] D.J. Stuckey, C.A. Carr, E. Martin-Rendon, D.J. Tyler, C. Willmott, P.J. Cassidy, S.J.M. Hale, J.E. Schneider, L. Tatton, S.E. Harding, G.K. Radda, S. Watt, K. Clarke, Stem Cells 24 (2006) 1968.
[4] L. Guczi, G. Stefler, O. Geszti, Zs. Koppány, Z. Kónya, É. Molnár, M. Urbán, I. Kiricsi, J. Catal. 244 (2006) 24.
[5] C.B. Wang, W.X. Zhang, Environ. Sci. Technol. 31 (1997) 2154.
[6] S.M. Ponder, J.G. Darab, T.E. Mallouk, Environ. Sci. Technol. 34 (2000) 2564.
[7] R.T. Wilkin, M.S. McNeil, Chemosphere 53 (2003) 715.
[8] L. Zhang, A. Manthiram, Nanostruct. Mater. 7 (1996) 437.
[9] S. Balakrishnan, M.J. Bonder, G.C. Hadjipanayis, J. Magn. Magn. Mater. 321 (2009) 117.
[10] L.T. Kuhn, A. Bojesen, L. Timmermann, M.M. Nielsen, S. Mørup, J. Phys.: Condens. Matter 14 (2002) 13551.
[11] E.E. Carpenter, S. Calvin, R.M. Stroud, V.G. Harris, Chem. Mater. 15 (2003) 3245.
[12] E.A. Shafranovsky, Y.I. Petrov, J. Nanopart. Res. 6 (2004) 71.
[13] C.M. Wang, D.R. Baer, L.E. Thomas, J.E. Amonette, J. Antony, Y. Qiang, G. Duscher, J. Appl. Phys. 98 (2005) 094308.
[14] F. Bergaya, B.K.G. Theng, G. Lagaly, Handbook of Clay Science, Developments in Clay Science, vol. 1, Elsevier, Amsterdam/London, 2006.
[15] B.Q. Chen, J.R.G. Evans, J. Phys. Chem. B 108 (2004) 14986.
[16] R.C. Mackenzie, J. Colloid Sci. 6 (1951) 219.
[17] K.C. Huang, S.H. Ehrman, Langmuir 23 (2007) 1419.
[18] K.C. Huang, K.S. Chou, Electrochem. Commun. 9 (2007) 1907.
[19] A. Corrias, G. Ennas, A. Musinu, G. Marongiu, G. Paschina, Chem. Mater. 5 (1993) 1722.
[20] D.J. Harris, T.J. Bonagamba, K. Schmidt-Rohr, Macromolecules 32 (1999) 6718.
[21] N. Aihara, K. Torigoe, K. Esumi, Langmuir 14 (1998) 4945.
[22] K.K. Fung, B.X. Qin, X.X. Zhang, Mater. Sci. Eng. A 286 (2008) 135.
[23] D.L. Leslie-Pelecky, R.D. Rieke, Chem. Mater. 8 (1996) 1770.
[24] J.I. Lai, K.V.P.M. Shafi, A. Ulman, K. Loos, Y. Lee, T. Vogt, W.L. Lee, N.P. Ong, J. Phys. Chem. B 109 (2005) 15.
[25] K. Racka, M. Gich, A. Ślawska-Waniewska, A. Roig, E. Molins, J. Magn. Magn. Mater. 290–291 (2005) 127.